Journal of Photochemistry and Photobiology A: Chemistry 206 (2009) 32–39

Contents lists available at ScienceDirect

Journal of Photochemistry and Photobiology A: Chemistry

journal homepage: www.elsevier.com/locate/jphotochem

Molecular assembly, physical characterization and photophysical properties of ternary lanthanide hybrids containing functional 1,2,4-triazole and 1,10-phenanthroline

Jinliang Liu, Bing Yan*

Department of Chemistry, Tongji University, Siping Road 1239 Shanghai 200092, PR China

ARTICLE INFO

Article history:
Received 19 December 2008
Received in revised form 13 April 2009
Accepted 11 May 2009
Available online 18 May 2009

Keywords:
Hybrid material
Chemically bonded
1,10-Phenanthroline
Photophysical property

ABSTRACT

This work focuses on the preparation and the study of the luminescence properties of series ternary lanthanide molecular hybrid materials. We selected 1,10-phenanthroline as a second ligand to introduce into the binary hybrid system in which an organic functional compound 1,2,4-triazole was included. The further investigation of the luminescence properties proves that, after the addition of the 1,10-phenanthroline, the energy levels matching degree between the organic segments and RE ions is more suited and appropriate so that the final ternary hybrid materials show stronger luminescence intensity, which substantiating that the heterocyclic ligand would become the main energy donor and has the possibility to sensitize Ln^{3+} ions via an intramolecular energy transfer process, at the same time, the luminescent quantum efficiencies of the ternary systems are also highly improved compared with the binary systems. Besides, the introduction of the second ligands don't change the disorder structure of the siliceous skeleton and thus no phase separation be observed in the hybrid systems. We may expect to obtain stable and efficient hybrid materials in optical or electronic areas from this method.

1. Introduction

Sol–gel derived organically modified silica materials have attracted a great deal of interests for photonic applications because they combine the thermal stability and the mechanical strength of the silica together with the optical characteristics of active organic complexes [1,2]. The introduction of the organic molecules or macromolecules into the Si–O–Si network allow the synthesis of bulk materials with adjustable properties [3,4], furthermore, the multifunctional alkoxysilanes makes it possible to create direct chemical bonds between the organic and inorganic components [5] and the as-derived molecular-based materials can exhibit monophasic appearance even at a high concentration of organic complexes.

Rare earth complexes have been well known as important components in luminescent materials owing to their excellent luminescent characteristics form the electronic transitions between the 4f energy levels. The luminescent mechanism is well known as an intramolecular energy transfer from the ligands to the metal ions, which is called the "antenna effect" [6–8]. However, the practical use of these complexes as luminescent devices has been restrained because of their pool photo and thermal stability and mechanical properties. To overcome these weaknesses, a few studies in terms of the constructing organic–inorganic hybrid materials by incorporating the rare earth complexes into a polymer matrix, especially the Si–O–Si matrix, have appeared [9,10]. According to the type of interactions between the organic and the inorganic components, the hybrids can be categorized into two main classes [11]: Class I materials concern the conventional doping systems in which only weak interactions (such as hydrogen bonding, van der Waals forces, or weak static effects) exist between organic and inorganic moieties. One way to obtain this kind of materials is to dope the silica gels with organometallic complexes. Inhomogeneous dispersion of two phases and leaching of the photoactive molecules frequently occur in this sort of hybrid materials. Class II materials belong to the molecule-based composite materials in which the organic and inorganic phases are linked together through strong chemical bonds (covalent, ion-covalent, or coordination bonds), and the as-derived molecular-based materials exhibit monophasic appearance even at a high concentration of rare earth complexes [12–19]. Moreover, the reinforcement of thermal and mechanical resistances has been clearly established.

Recently we have synthesized a family of organic–inorganic molecular hybrid materials containing functional triazole heterocyclic organic components [20]. And the intramolecular energy transfer mechanism between the organic triazole heterocyclic ligand with the RE ions was investigated. However, a key issue that remains in these organic modified materials is that the

* Corresponding author. Tel.: +86 21 65984663; fax: +86 21 65982287.
E-mail address: byan@tongji.edu.cn (B. Yan).

1010-6030/$ – see front matter © 2009 Elsevier B.V. All rights reserved.
doi:10.1016/j.jphotochem.2009.05.009

luminescence lifetimes and the quantum yields of the emission in these kinds of hybrids are much lower. This may be because the radiative transition of RE ions incorporated into the sol–gel derived Si–O–Si matrices can be quenched due to coupling with the vibrations of their environments, in particular with the –OH groups of Si–OH and H_2O molecule. Moreover, the energy levels matching degree between the organic segments and RE ions may be not suited and appropriate. In order to solve this problem, in this study, we introduced 1,10-phenanthroline as a second ligand to coordinate with the RE ions and a series of ternary hybrid systems were presented. Compared with the binary hybrid systems, we can see that the presence of the second ligand 1,10-phenanthroline in the ternary hybrid systems can prevent the quenching of the emission of RE ions, decreased the spectral width and increased the decay time as well as the emission intensity of the RE ions, and thus improve the quantum yields of the hybrids.

2. Experimental

2.1. Physical measurements

FT-IR spectra (KBr) were measured within the 4000–400 cm^{-1} region on a Nicolet model 5SXC spectrophotometer. The X-ray diffraction (XRD) measurements were carried out on powdered samples via a BRUKER D8 diffractometer (40 mA/40 kV) using monochromated $CuK_{\alpha1}$ radiation (λ = 1.54 Å) over the 2θ range of

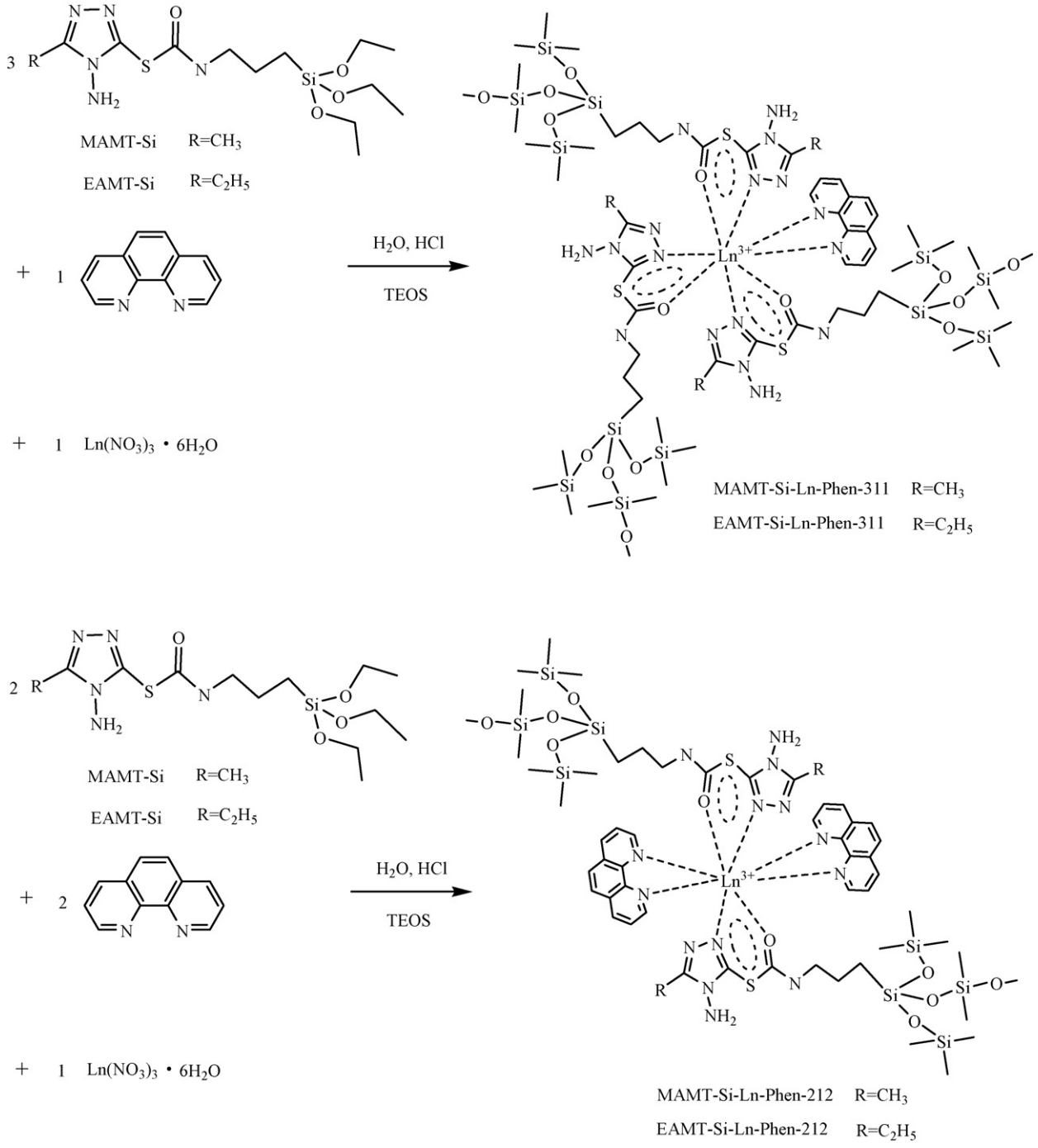

Fig. 1. Scheme of the synthesis process of the hybrid materials MAMT-Si-Ln-Phen-311, MAMT-Si-Ln-Phen-212, EAMT-Si-Ln-Phen-311 and EAMT-Si-Ln-Phen-212.

10°–70°. Differential scanning calorimetry (DSC) and thermogravimetric analysis (TGA) were performed on a NETZSCH STA 449C with a heating rate of 10 K/min under a nitrogen atmosphere (flow rate: 40 mL/min). Scanning electronic microscope (SEM) images were obtained with a Philips XL-30. Reflectivity spectra were recorded on a Bws003 spectrometer equipped with a diffuse reflectance accessory. Fluorescence excitation and emission spectra were obtained on a RF-5301 spectrophotometer with 1.5 nm excitation and 1.5 nm emission slits. Luminescent lifetimes were recorded on an Edinburgh FLS 920 phosphorimeter using a 450 W xenon lamp as excitation source (pulse width, 3 μs).

2.2. Materials

Europium and Terbium nitrates were obtained from their corresponding oxides in concentrated nitric acid. Tetraethoxysilane (TEOS) was distilled and stored under a N_2 atmosphere. The solvents were purified before been used. Other starting reagents were used as received.

2.3. Synthesis

The organic compounds 3-alkyl-4-amino-5-mercapto-1,2,4-triazole (MAMT and EAMT) and the silylated precursors (MAMT-Si and EAMT-Si) were synthesized using a procedure described previously [20]. The hybrid materials (MAMT-Si-Ln-Phen-311, MAMT-Si-Ln-Phen-212, EAMT-Si-Ln-Phen-311, EAMT-Si-Ln-Phen-212) were prepared according to the procedure depicted in Fig. 1.

A typical procedure for the preparation of the hybrid materials was as follows. 2 mmol of the precursor (MAMT-Si or EAMT-Si) was dissolved in 20 mL of absolute ethanol, the solution was warmed to 40 °C, then a stoichiometric amount of $Ln(NO_3)\cdot 6H_2O$ and 1,10-phenanthroline were added. The resulting mixture was kept warmly about 5 h with stirring. After that TEOS and H_2O were added warmly. The mole ratio of Precursor (MAMT-Si or EAMT-Si)/$Ln(NO_3)\cdot 6H_2O$/1,10-phenanthroline/TEOS/H_2O was 3:1:1:6:24 for MAMT-Si-Ln-Phen-311 (EAMT-Si-Ln-Phen-311), and 2:1:2:4:16 for MAMT-Si-Ln-Phen-212 (EAMT-Si-Ln-Phen-212). After the addition, one drop of diluted hydrochloric acid was added to the final stirring mixture to promote hydrolysis. After the individual hydrolysis of the silylated precursors and TEOS, an appropriate amount of hexamethylene-tetramine was added to adjust the pH value of 6–7, and the polycondensation reactions between hydroxyl groups of both the silylated precursors and TEOS would take place. The resulting mixture was agitated magnetically to achieve a single phase and thermal curing was performed at 60 °C in a covered Teflon beaker for about 6 days until the sample solidified. The obtained molecular hybrid materials were collected as monolithic bulks and then washed with ethanol and dried at 80 °C for about 2 days. The final materials were ground into powdered material for the photophysical studies.

3. Results and discussion

3.1. FT-IR spectra

All of the obtained hybrid materials were characterized by infrared spectroscopy. The IR spectra of (A) MAMT-Si-Eu-Phen-311, (B) MAMT-Si-Tb-Phen-311, (C) MAMT-Si-Eu-Phen-212, (D) MAMT-Si-Tb-Phen-212 are shown in Fig. 2. The most obvious bands located at 1317, 1385, 1485, 1505 cm^{-1}, originating from the 1,10-phenanthroline group, are growing stronger in the MAMT-Si-Ln-Phen-212 hybrids when the amount of the 1,10-phenanthroline are larger. The broad absorptions of the (ν(Si–O–Si)) vibration located in 1109–1040 cm^{-1} wavelength ranges can be seen in all

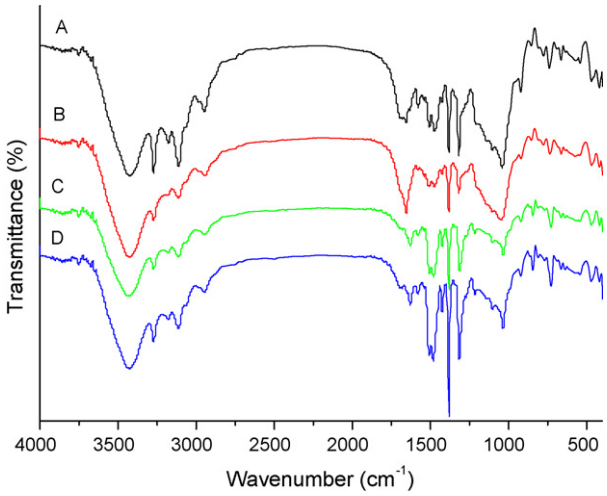

Fig. 2. Infrared spectra of the hybrid materials (A) MAMT-Si-Eu-Phen-311, (B) MAMT-Si-Tb-Phen-311, (C) MAMT-Si-Eu-Phen-212, (D) MAMT-Si-Tb-Phen-212 in the 4000-400 cm^{-1} range.

of the spectra, which can indicate the formation of Si–O–Si network during the hydrolysis/condensation reactions. The presence of the ν(Si–C) absorption located in 1200–1192 cm^{-1} wavelength ranges is consistent with the fact that no (Si–C) bond cleavage occurs [13]. Further, the accomplishment of the coordination reaction of Ln^{3+} can be clearly shown by infrared spectroscopy. The ν(C=O) vibrations of the –CONH– groups and the ν(C=N) vibrations of the 1,2,4-triazole groups are shifted to lower frequency ($\Delta\nu$ = 10–40 cm^{-1}), This is ascribe to the complexation of the Ln^{3+} ion with the silylated precursors in hybrids [13,20]. Meanwhile, the twisting bending vibrations at 854 and 740 cm^{-1} which belong to the absorption of hydrogen atoms of 1,10-phenanthroline have almost disappeared, this fact firmly prove that the 1,10-phenanthroline can effectively coordinate to the rare earth ions [21]. The formation of H_2O molecule during the hydrolysis/condensation reactions can also be clearly indicated by the IR spectra. The vibration signal around 3400 cm^{-1}, which is the most intense in the spectra, together with the presence of a signal in around 1628 cm^{-1}, is the characteristic of H_2O molecule. Likewise, the IR spectra of EAMT-Si hybrid systems (not given) present similar results.

3.2. Powder XRD

The X-ray diffraction patterns of the hybrid materials MAMT-Si-Ln-Phen-311, MAMT-Si-Ln-Phen-212, EAMT-Si-Ln-Phen-311, EAMT-Si-Ln-Phen-212 are reproduced in Fig. 3. In general, when a material contains a large crystalline region, the peak observed is usually sharp and its intensity is strong, whereas that of amorphous material is rather broad [22]. From the spectra we can see that all the materials are totally amorphous. All the diffraction curves show the similar broad peaks, with angel 2θ centered around 22.3°, which are characteristic of amorphous silica materials [23]. Compared with the previous work we have done [20], it seems that the introducing of the second ligand (1,10-phenanthroline) has not changed the disorder structure of the siliceous skeleton. The structural unit distance, calculated using the Bragg law, is approximately 3.98 Å, a little bigger than the hybrids in which 1,10-phenanthroline was not included (3.83 Å). This may be ascribed to the coherent diffraction of the siliceous backbone of the hybrids [24,25], the second ligand did not influence the backbone of the hybrids much. The absence of any crystalline regions in these samples is due to the presence of organic chains in the host inorganic framework [26]. In addition, none of the hybrid materials contains

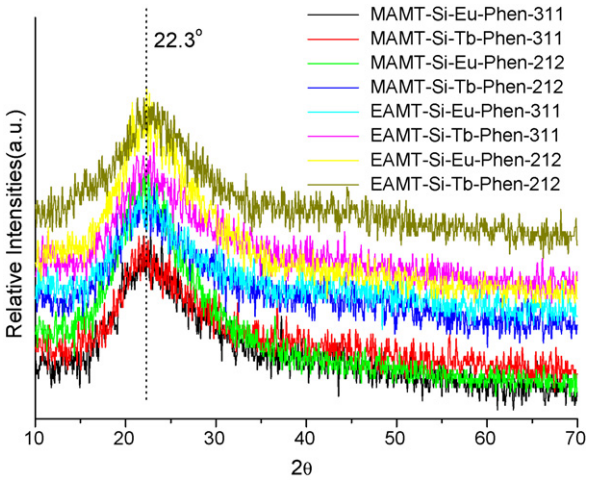

Fig. 3. The X-ray diffraction (XRD) graphs of the hybrids MAMT-Si-Ln-Phen-311, MAMT-Si-Ln-Phen-212, EAMT-Si-Ln-Phen-311 and EAMT-Si-Ln-Phen-212.

measurable amounts of phases corresponding to the pure organic compound (silylated precursors MAMT-Si and EAMT-Si or 1,10-phenanthroline) or free RE nitrate, which is an initial indication for the formation of the true covalent-bonded molecular hybrid materials.

3.3. Differential scanning calorimetry (DSC) and thermogravimetric analysis (TGA)

Differential scanning calorimetry (DSC) and thermogravimetric analysis (TGA) were performed to examine the thermal activities of the hybrid materials. Fig. 4 shows the TGA and DSC traces of the hybrids MAMT-Si-Tb-Phen-311, MAMT-Si-Tb-Phen-212, EAMT-Si-Tb-Phen-311 and EAMT-Si-Eu-Phen-212. From the curves we can see that, all the samples show the similar change trends in weight losses, and two main degradation steps can be obviously found. The first weight loss between 200 and 400 °C was attributed to the thermal degradation of the organosilicate framework, involving Si–C, C–C, and C–N bond cleavage [27]. Whereas the slight weight loss beyond 400 °C was ascribed to the release of water formed from the further condensation of silanols in the silica framework. Because there are even some Si–OH groups on the silica surface and these

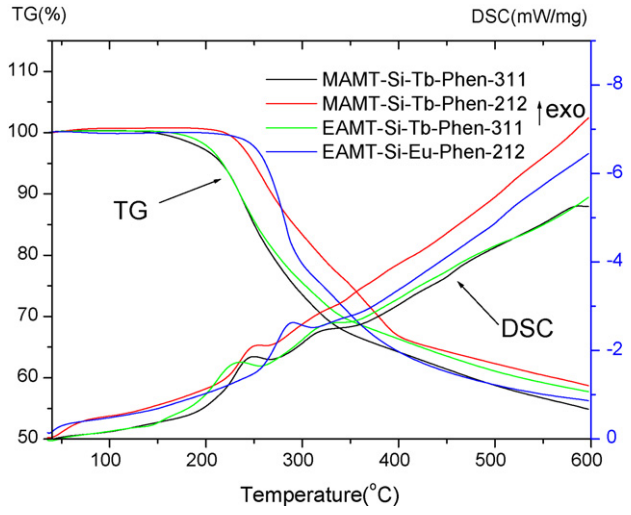

Fig. 4. The DSC and TGA traces of MAMT-Si-Tb-Phen-311, MAMT-Si-Tb-Phen-212, EAMT-Si-Tb-Phen-311 and EAMT-Si-Eu-Phen-212.

groups have the ability to undergone condensation to form Si–O–Si networks with the increasing treatment temperature. The thermal stability of the ternary hybrids is higher enhanced than that of binary systems and the weight losses under 200 °C are disappeared, This may because the second ligand 1,10-phenanthroline has taken the place of the coordination H_2O molecule and a more stable coordination structures were formed thus enhanced the thermal activities. The slight differences (<2%) of the weight losses for them may be due to the different organic silylated precursors (MAMT-Si or EAMT-Si) and the different degrees of the polycondensation reactions. Otherwise, the MAMT-Si-Tb-Phen-212 and the EAMT-Si-Eu-Phen-212 hybrids show an improved thermal stability (about 40 °C in degradation temperature) than the MAMT-Si-Tb-Phen-311 and the EAMT-Si-Tb-Phen-311 hybrids. This may be due to the coordination modality of the hybrid systems. Because the second ligand 1,10-phenanthroline has an excellent coordination capability to rare earth ions and the larger amount of the addition in MAMT-Si-Tb-Phen-212 and the EAMT-Si-Eu-Phen-212 systems may proved a more stable coordination structures and thus affect the thermal activities. However, it seems that the exchange of the Eu^{3+} ions or Tb^{3+} ions has no influence on the thermal stabilities of the hybrids. This might be due to the structures of the siliceous skeleton were not changed. Likewise, The MAMT-Si-Eu-Phen-311, MAMT-Si-Eu-Phen-212, EAMT-Si-Eu-Phen-311 and EAMT-Si-Tb-Phen-212 hybrid systems present similar results.

3.4. Scanning electron micrograph (SEM)

Fig. 5 shows the selected micrographs for (A) MAMT-Si-Tb-Phen-311, (B) EAMT-Si-Tb-Phen-311, (C) MAMT-Si-Tb-Phen-212, (D) EAMT-Si-Eu-Phen-212. In most cases, surface morphology of materials is of great importance for many technical applications requiring well-defined surface or interfaces. From the figure we can see that all the samples show a homogeneous system and no phase separation could be observed. That may because the covalent bonding (Si–O–Si) enhanced the miscibility of the organic compounds and the silica matrixes, so the inorganic and the organic phases can exhibit their distinct properties together via a self-assemble process during the hydrolysis/polycondensation process. Basically, the sol–gel synthesis of organic-silica hybrid materials mainly involves three steps, that is, hydrolysis, condensation and polycondensation [28], these three steps cannot be totally isolated, and they proceed in parallel rather than in sequence. Their relative rates determine the final structure of the wet silica gel [29]. There are many granules on the surface of the MAMT-Si-Tb-Phen-311 and EAMT-Si-Tb-Phen-311 hybrids, while in MAMT-Si-Tb-Phen-212 and EAMT-Si-Eu-Phen-212 hybrids, the granules become bigger and some scale like microstructure can be observed. This may be attributed to the condensation reaction, which takes place between ethoxy–ethoxy, silanol–silanol and ethoxy–silanol groups, leading to the formation of siloxane chains. Meanwhile, the different degree of the polycondensation reaction caused the different sizes of the granules in the surface of the hybrids. Furthermore, the further hydrolysis of the remaining alkoxy groups and polycondensation (or gelation) between chains gives rise to a three-dimensional, cross-linked solid network of siloxane (Si–O–Si), which is an indication for the formation of the network structures seeing from the MAMT-Si-Tb-Phen-311 and EAMT-Si-Tb-Phen-311 hybrids. For MAMT-Si-Tb-Phen-212 and EAMT-Si-Eu-Phen-212 hybrids, it is indicated that the tendency to form one-dimensional chain-like structure after the more addition of the second ligand has become the important tendency competed with the tendency to form the polymeric Si–O–Si network, which forms the final dendritic stripe microstructure that can be seen from the SEM of the EAMT-Si-Eu-Phen-212 hybrids obviously.

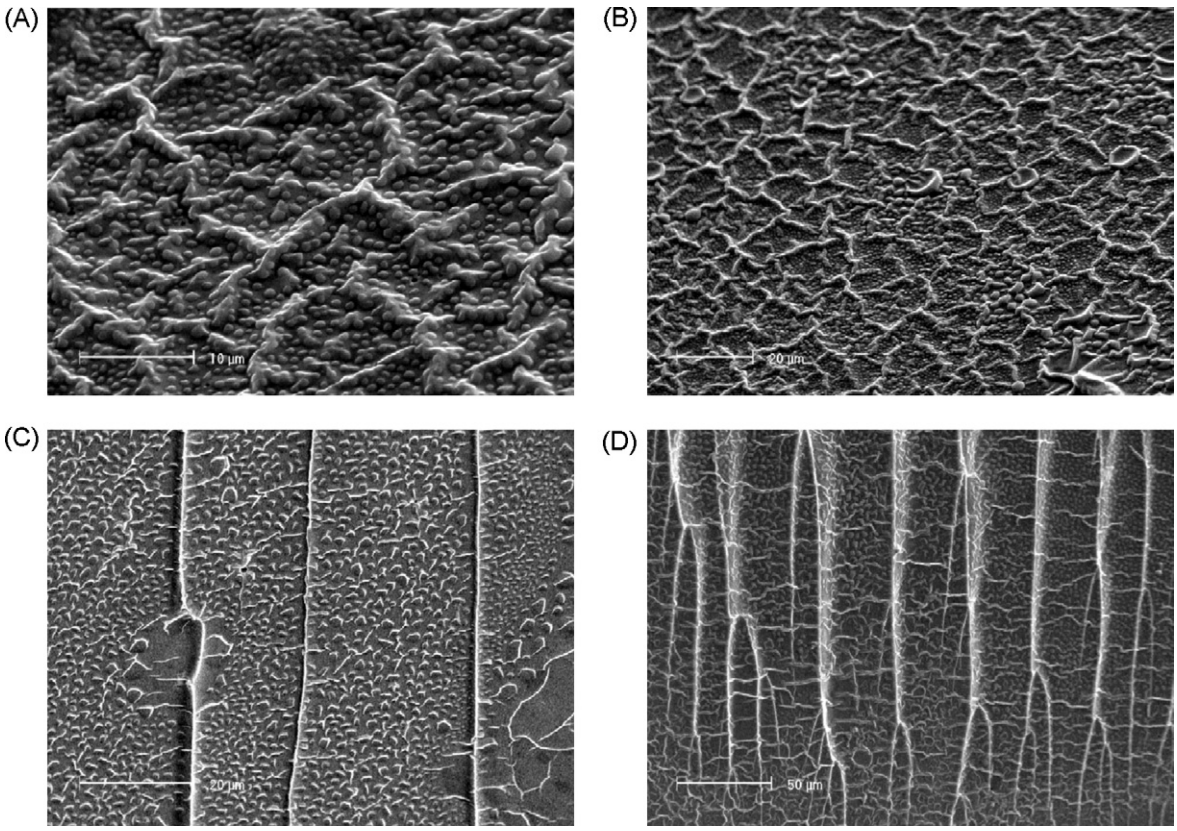

Fig. 5. SEM images for molecular-based hybrid materials with organic and inorganic networks, (A) MAMT-Si-Tb-Phen-311, (B) EAMT-Si-Tb-Phen-311, (C) MAMT-Si-Tb-Phen-212, (D) EAMT-Si-Eu-Phen-212.

3.5. Diffuse reflectivity spectra

Diffuse reflectance experiments were performed on all of the powdered materials and the corresponding absorption spectra of (A) MAMT-Si-Eu-Phen-311, MAMT-Si-Eu-Phen-212, EAMT-Si-Eu-Phen-311, EAMT-Si-Eu-Phen-212 and (B) MAMT-Si-Tb-Phen-311, MAMT-Si-Tb-Phen-212, EAMT-Si-Tb-Phen-311, EAMT-Si-Tb-Phen-212 are shown in Fig. 6. All of the spectra exhibit the similar broad absorption bands in the UV–vis range (220–350 nm), which partially overlap with the fluorescence excitation spectra (wide bands at 250–380 nm in Fig. 7(A) and (B)). This absorption band may correspond to transition from the ground states of the organic ligands to the first excited states ($S_0 \rightarrow S_1$). It is more specifically attributed to $\pi \rightarrow \pi^*$ transition of the 1,2,4-triazole group and the 1,10-phenanthroline group. Compared with the hybrid systems we have reported previously [20], a red shift is observed in the spectra after the introduction of the 1,10-phenanthroline. According to Dexter's exchange energy transfer theory, the intramolecular energy transfer efficiency mainly depends on the matching degree between the ligand's triplet state energy and lanthanide iron's emission energy and thus influence the luminescence intensity of hybrid material. Established on this theory we can primarily predicted that, energy transfer process will occur from MAMT (or EAMT) to 1,10-phenanthroline, substantiating that the heterocyclic ligand will become the main energy donor and have the possibility to sensitize Ln^{3+} ions. Furthermore, after the introduction of second ligand 1,10-phenanthroline, the organic segments can absorb more abundant energy in ultraviolet-visible extent and the energy levels matching degree between the organic segments and RE ions is more suited and appropriate so that the final ternary hybrid materials can be expected to have strong luminescence via an intramolecular energy transfer process, which can be proved by the intension of the emission peaks in 450–700 nm ranges. Meanwhile, the signals of 591, 614, 685 nm in Fig. 6(A) and 490, 545 nm in Fig. 6(B) were also observed in the spectra, which due to the corresponding Eu^{3+} and Tb^{3+} ions, respectively. For MAMT-Si-Ln-Phen-212 and EAMT-Si-Ln-Phen-212 hybrid systems, the intensities of the signals are largely improved compared with the MAMT-Si-Ln-Phen-311 and EAMT-Si-Ln-Phen-311 hybrid systems. It is indicated that the addition of the second ligand 1,10-phenanthroline can largely sensitize the emission of rare earth ions, this can also be proved by the fluorescence spectra in Fig. 7(A). However, for terbium hybrid systems, the intensities of the signals are not largely different, which mean the sensitization effect for terbium ions is not obviously compared with europium ions. Even so, the sensitization effect can also be obviously seen from the fluorescence spectra in Fig. 7(B).

3.6. Photoluminescence properties

Fig. 7 shows the excitation and emission spectra of the europium hybrid materials (A) MAMT-Si-Eu-Phen-311, MAMT-Si-Eu-Phen-212, EAMT-Si-Eu-Phen-311, EAMT-Si-Eu-Phen-212 and the terbium hybrid materials (B) MAMT-Si-Tb-Phen-311, MAMT-Si-Tb-Phen-212, EAMT-Si-Tb-Phen-311, EAMT-Si-Tb-Phen-212. From the spectra we can see that, excellent emissions of lanthanide ions were obtained because the introduction of the second ligand 1,10-phenanthroline. The excitation spectra were obtained by monitoring the emission of Eu^{3+} or Tb^{3+} at 614 or 545 nm. For Eu^{3+} hybrids, all the systems have similar excitation spectra that are dominated by a broad band from 250 to 380 nm with the maximum peak at about 330 nm. As a result, the emission lines of the hybrid materials were assigned to the characteristic $^5D_0 \rightarrow {}^7F_1$ and $^5D_0 \rightarrow {}^7F_2$ transitions at 590 and 614 nm, respectively, while the emission lines of $^5D_0 \rightarrow {}^7F_3$ and $^5D_0 \rightarrow {}^7F_4$ are too weak to be observed. The $^5D_0 \rightarrow {}^7F_2$ emission around 614 nm is the most predominant transition, which agrees with the amorphous char-

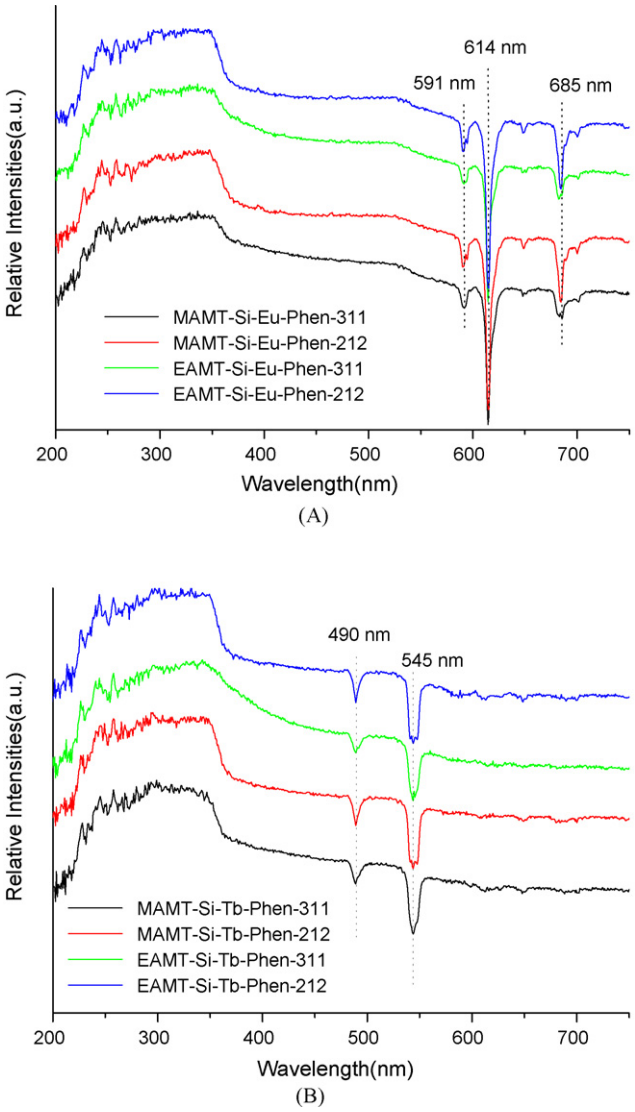

Fig. 6. The ultraviolet-visible diffuse reflection absorption spectra of europium hybrid materials (A) MAMT(EAMT)-Si-Eu-Phen-311, MAMT(EAMT)-Si-Eu-Phen-212, and the terbium hybrid materials (B) MAMT(EAMT)-Si-Tb-Phen-311, MAMT(EAMT)-Si-Tb-Phen-212.

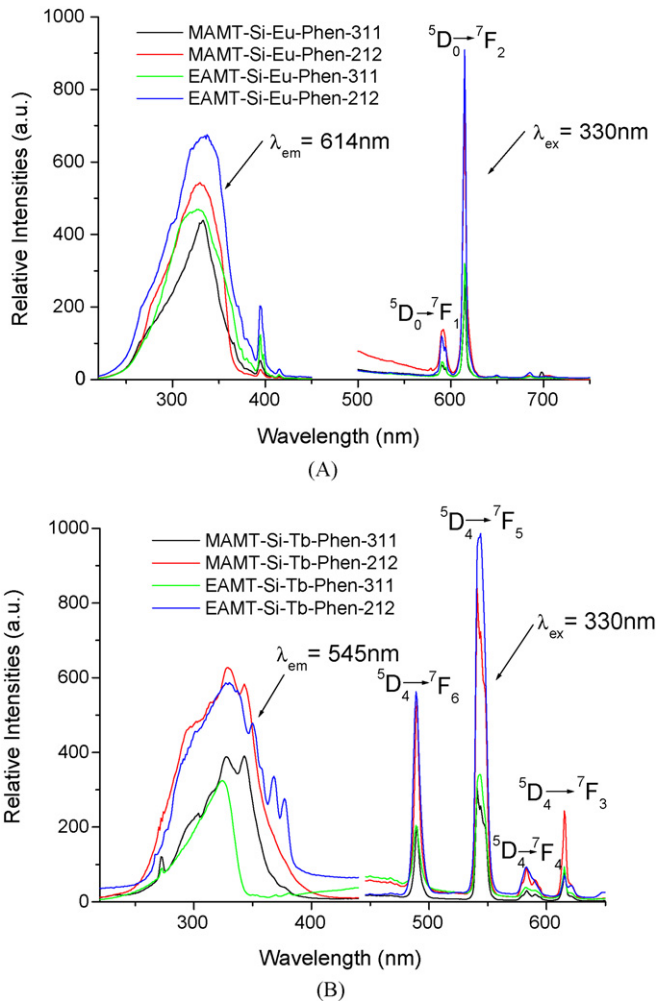

Fig. 7. The excitation and emission spectra of the europium hybrid materials (A) MAMT(EAMT)-Si-Eu-Phen-311, MAMT(EAMT)-Si-Eu-Phen-212, and the terbium hybrid materials (B) MAMT(EAMT)-Si-Tb-Phen-311, MAMT(EAMT)-Si-Tb-Phen-212.

acters of the hybrid materials. From the spectra, we can see that the fluorescence emission intensities of these kinds of materials are determined in the order: EAMT-Si-Eu-Phen-212 > MAMT-Si-Eu-Phen-212 > EAMT-Si-Eu-Phen-311 > MAMT-Si-Eu-Phen-311, which indicate that the second ligand 1,10-phenanthroline can efficiently sensitize the luminescence of Eu^{3+} ions, the more the amount of the 1,10-phenanthroline are added, the stronger the intension of the fluorescence emissions of the hybrids are. From the spectra we can also see that, the exchange of the silylated precursors (MAMT-Si and EAMT-Si) has nearly no influence on the fluorescence emission intensities. This can also prove that the 1,10-phenanthroline become the main energy donor and the effective energy transfer take place between the MAMT-Si-Phen (or EAMT-Si-Phen) with the chelated Eu3$^+$ ions. For Tb^{3+} hybrids, a broad band centered at around 330 nm was observed in the excitation spectra and as a result, the emission lines were assigned to the $^5D_4 \rightarrow ^7F_J$ transitions located at 490, 544, 587 and 622 nm, for J = 6, 5, 4 and 3 respectively. The most striking green fluorescence ($^5D_4 \rightarrow ^7F_5$) was observed due to the fact that this emission is the most intense one. Corresponding to the emission spectra of Eu^{3+} hybrids, the fluorescent intensities of Tb^{3+} hybrids change with the same sequence, that is EAMT-Si-Tb-Phen-212 > MAMT-Si-Tb-Phen-212 > EAMT-Si-Tb-Phen-311 > MAMT-Si-Tb-Phen-311. Compared with the binary hybrid systems we have reported previously [20], the fluorescence intensities of molecular hybrids are much enhanced when the second ligands are added to the hybrids, especially for the addition of 1,10-phenanthroline. This is a good method to prepare materials with strong luminescence emissions.

3.7. *Luminescence decay times (τ) and Emission quantum efficiency (η)*

The typical decay curves of the ternary europium hybrid materials were measured using a selective excitation wavelength of 330 nm, and they can be described as a single exponential ($\mathrm{Ln}(S(t)/S_0) = -k_1 t = -t/\tau$), indicating that all Eu^{3+} ions occupy the same average coordination environment. The typical decay curve of the MAMT-Si-Eu-Phen-311 hybrid material is shown in Fig. 8 as an example and the resulting lifetimes of Eu^{3+} hybrids were given in Table 1. The influence of 1,10-phenanthroline can be illustrated by comparing the ternary systems with the corresponding binary systems reported previously [20]. The Eu^{3+} lifetimes in ternary hybrid materials are much longer than those in the corresponding binary materials, this may be ascribed to the reducing of the quenching effect by –OH– group from the coordinated H_2O after the introduction of the second ligand 1,10-phenanthroline. In addition, the

Table 1
The luminescence efficiencies and lifetimes for the europium hybrid materials MAMT-Si-Eu-Phen-311, MAMT-Si-Eu-Phen-212, EAMT-Si-Eu-Phen-311 and EAMT-Si-Eu-Phen-212.

Hybrids	υ_{01} (cm^{-1})[a]	υ_{02} (cm^{-1})[a]	A_{0J} (s^{-1})	A_r (s^{-1})	A_{nr} (s^{-1})	τ (μs)[b]	η (%)
MAMT-Si-Eu-Phen-311	16978	16313	50,371	421	603	977	41.1
MAMT-Si-Eu-Phen-212	16978	16313	50,257	307	787	914	28.1
EAMT-Si-Eu-Phen-311	16978	16313	50,332	382	629	989	37.8
EAMT-Si-Eu-Phen-212	16978	16313	50,401	451	604	948	42.7

[a] The energies of the $^5D_0 \rightarrow {}^7F_J$ transitions (υ_{0J}).
[b] For $^5D_0 \rightarrow {}^7F_2$ transition of Eu^{3+}.

energy levels matching degree between the organic segments and RE ions is more suited and appropriate as the 1,10-phenanthroline become the main energy donor and thus reduces the non-radiative energy loss compared with the binary systems.

According to the emission spectrum and the lifetime of the Eu^{3+} first excited level (τ, $^5D_0$), the emission quantum efficiency (η) of the $^5D_0$ Eu^{3+} excited state can be determined, and the detailed luminescent data was shown in Table 1. On the basis of the emission spectra and lifetimes of the $^5D_0$ emitting level, we selectively determined the emission quantum efficiencies of the $^5D_0$ excited state of europium ion for Eu^{3+} hybrids. Assuming that only non-radiative and radiative processes are essentially involved in the depopulation of the $^5D_0$ state, the quantum efficiency of the luminescence step, η can be defined as how well the radiative processes compete with non-radiative processes, the detailed principles and methods were adopted from Refs [30–38].

$$\eta = \frac{A_r}{A_r + A_{nr}} \quad (1)$$

$$\tau_{exp} = (A_r + A_{nr})^{-1} \quad (2)$$

$$\eta = A_r \tau_{exp} \quad (3)$$

$$A_r = \Sigma A_{0J} = A_{00} + A_{01} + A_{02} + A_{03} + A_{04} \quad (4)$$

$$A_{0J} = A_{01}\left(\frac{I_{0J}}{I_{01}}\right)\left(\frac{\upsilon_{01}}{\upsilon_{0J}}\right) \quad (5)$$

where A_r and A_{nr} are radiative and non-radiative transition rates, respectively. A_r can be obtained by summing over the radiative rates A_{0J} for each $^5D_0 \rightarrow {}^7F_J$ transitions of Eu^{3+} [30–38]. Since $^5D_0 \rightarrow {}^7F_1$ belongs to the isolated magnetic dipole transition, it is practically independent of the chemical environments around the Eu^{3+} ion, and thus can be considered as an internal reference for the whole spectrum, A_{0J} is the experimental coefficients of spontaneous emissions, among A_{01} is the Einstein's coefficient of spontaneous emission between the $^5D_0$ and $^7F_1$ energy levels. In vacuum, the value of A_{01} can be determined to be 50 s^{-1} approximately ($A_{01} = n^3 A_{01\ (vacuum)}$) [38]. I is the emission intensity and can be taken as the integrated intensity of the $^5D_0 \rightarrow {}^7F_J$ emission bands [37,38]. υ_{0J} refers to the energy barycenter and can be determined from the emission bands of Eu^{3+}'s $^5D_0 \rightarrow {}^7F_J$ emission transitions. Here the emission intensity I, taken as integrated intensity S of the $^5D_0 \rightarrow {}^7F_{0-4}$ emission curves.

From the discussion mentioned above, it can be seen the value η mainly depends on the values of two quanta: one is lifetime and the other is I_{02}/I_{01} (red/orange ratio). If the lifetimes and red/orange ratio are large, the quantum efficiency must be high. As shown in Table 1, the ternary hybrid systems exhibit much higher quantum efficiencies than the binary hybrid systems, this finding agrees with the results from the luminescent intensities and lifetimes. So we can see that the addition of the second ligand into the hybrids not only enhance the materials' luminescent intensities, but also extend the materials' luminescent lifetimes and thus improve the materials' quantum efficiencies.

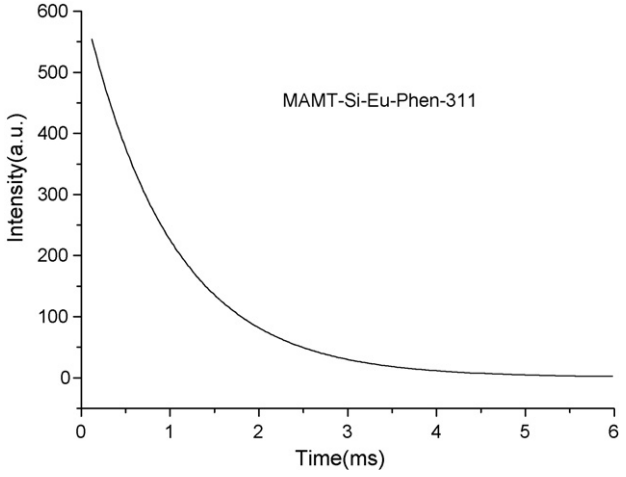

Fig. 8. The decay curves of MAMT-Si-Eu-Phen-311 hybrid material.

4. Conclusion

In summary, in order to obtain luminescent materials with stronger luminescent intensities as well as higher emission quantum efficiency, we successfully prepared a series of ternary lanthanide molecular hybrid materials containing functional 1,2,4-triazole and 1,10-phenanthroline organic segment. Measurements of the photoluminescent properties of these materials show that the ternary rare earth/inorganic/organic hybrids present stronger luminescent intensities, longer lifetimes, and higher luminescent quantum efficiencies than the binary hybrids, indicating that the introduction of the second ligand can sensitize the luminescence emission of the overall hybrid system. In addition, all of these ternary hybrid materials exhibit homogeneous microstructures and morphologies, suggesting the introduction of the second ligand does not change the structure of the siliceous skeleton and the self-assembly process occur between the inorganic network and organic chain. As the synthesis process can be easily applied to other binary systems, we may expect to obtain stable and efficient hybrid materials in optical or electronic areas for the desired properties can be tailored by an appropriate choice of the precursors and the addition of the second ligand.

Acknowledgement

This work was supported by the National Natural Science Foundation of China (20671072) and Program for New Century Excellent Talents in University (NCET-08-0398).

References

[1] A.B. Seddon, Sol-gel derived organic–inorganic hybrid materials for photonic applications, IEE Proc. Circuits Devices Syst. 145 (1998) 369–372.
[2] E.J.A. Pope, Sol-gel optical nanocomposites: design and applications, J. Sol-Gel Sci. Technol. 2 (1994) 717–722.

[3] X.C. Li, T.A. King, Structural modification of sol-gel-derived optical composites, SPIE Sol-Gel Opt. III 2288 (1994) 216–226.
[4] J. Wen, G.L. Wilkes, Organic/inorganic hybrid network materials by the sol-gel approach, Chem. Mater. 8 (1996) 1667–1681.
[5] L.S. Fu, H.J. Zhang, S.B. Wang, Q.G. Meng, K.Y. Yang, J.Z. Ni, Preparation and luminescence properties of the ternary europium complex incorporated into an inorganic/polymer matrix by a sol-gel method, J. Sol-Gel Sci. Technol. 15 (1999) 49–55.
[6] S.I. Klink, L. Grave, D.N. Reinhoudt, F.C.J.M. van Veggel, M.H.F. Werts, F.A.J. Geurts, J.W. Hofstraat, A systematic study of the photophysical processes in polydentate triphenylene-functionalized Eu^{3+}, Tb^{3+}, Nd^{3+}, Yb^{3+}, and Er^{3+} complexes, J. Phys. Chem. A 104 (2000) 5457–5468.
[7] N.S. Baek, Y.H. Kim, S.G. Roh, B.K. Kwak, H.K. Kim, The first inert and photostable encapsulated lanthanide(III) complexes based on dendritic 9,10-diphenylanthracene ligands, synthesis, strong near-infrared emission enhancement, and photophysical studies, Adv. Funct. Mater. 16 (2006) 1873–1882.
[8] Q.M. Wang, B. Yan, Novel luminescent terbium molecular-based hybrids with modified meta-aminobenzoic acid covalently bonded with silica, J. Mater. Chem. 14 (2004) 2450–2454.
[9] O.A. Serra, E.J. Nassar, I.L.V. Rosa, Tb^{3+} molecular photonic devices supported on silica gel and functionalized silica gel, J. Lumin. 72–74 (1997) 263–265.
[10] M. Bredol, U. Kynast, M. Boldhaus, C. Lau, Luminescent inorganic networks, Ber. Bunsen-Ges. Phys. Chem. 102 (1998) 1557–1560.
[11] H.R. Li, J. Lin, H.J. Zhang, L.S. Fu, Preparation and luminescence properties of hybrid materials containing europium(III) complexes covalently bonded to a silica matrix, Chem. Mater 14 (2002) 3651–3655.
[12] D.W. Dong, S.C. Jiang, Y.F. Men, X.L. Ji, B.Z. Jiang, Nanostructured hybrid organic-inorganic lanthanide complex films produced in situ via a sol-gel approach, Adv. Mater. 12 (2000) 646–649.
[13] A.C. Franville, D. Zambon, R. Mahiou, Luminescence behavior of sol-gel-derived hybrid materials resulting from covalent grafting of a chromophore unit to different organically modified alkoxysilanes, Chem. Mater. 12 (2000) 428–435.
[14] B. Yan, H.F. Lu, Lanthanide-centered covalently bonded hybrids through sulfide linkage, molecular assembly, physical characterization, and photoluminescence, Inorg. Chem. 47 (2008) 5601–5611.
[15] H.R. Li, J. Lin, H.J. Zhang, L.S. Fu, Novel, covalently bonded hybrid materials of europium (terbium) complexes with silica, Chem. Commun. (2001) 1212–1213.
[16] Q.M. Wang, B. Yan, A Novel Way to Prepare Luminescent Terbium Molecular-Scale Hybrid Materials, Modified Heterocyclic Ligands Covalently Bonded with Silica, Crystal Growth & Design 5 (2005) 497–503.
[17] B. Yan, Q.M. Wang, Two luminescent molecular hybrids composed of bridged Eu(III)-b-Diketone chelates covalently trapped in silica and titanate gels, Crystal Growth & Design 8 (2008) 1484–1489.
[18] J.L. Liu, B. Yan, Lanthanide (Eu^{3+}, Tb^{3+}) centered hybrid materials using modified functional bridge chemical bonded with silica: molecular design, physical characterization, and photophysical properties, J. Phys. Chem. B 112 (2008) 10898–10907.
[19] Y. Li, B. Yan, H. Yang, Construction, characterization, and photoluminescence of mesoporous hybrids containing europium(III) complexes covalently bonded to SBA-15 directly functionalized by modified β-Diketone, J. Phys. Chem. C 112 (2008) 3959–3968.
[20] J.L. Liu, B. Yan, Molecular construction and photophysical properties of luminescent covalently bonded lanthanide hybrid materials obtained by grafting organic ligands containing 1,2,4-triazole on silica by mercapto modification, J. Phys. Chem. C 112 (2008) 14168–14178.
[21] Q.M. Wang, B. Yan, X.H. Zhang, Photophysical properties of novel lanthanide complexes with long chain mono-eicosyl cis-butene dicarboxylate, J. Photochem. Photobiol. A 174 (2005) 119–124.
[22] J.H. Kim, Y.M. Lee, Gas permeation properties of poly(amide-6-b-ethyleneoxide)-silica hybrid membranes, J. Membr. Sci. 193 (2001) 209–225.
[23] H.S. Hoffmann, P.B. Staudt, T.M.H. Costa, C.C. Moro, E.V. Benvenutti, FTIR study of the electronic metal-support interactions on platinum dispersed on silica modified with titania, Surf. Interface Anal. 33 (2002) 631–634.
[24] L.D. Carlors, V. de, Zea. Bermudez, R.A. Sá Ferreira, L. Marques, M. Assunção, Sol-gel derived urea cross-linked organically modified silicates. 2 blue-light emission, Chem. Mater. 11 (1999) 581–588.
[25] M.C. Goncalves, V. de, Zea. Bermudez, R.A. Sá Ferreira, L.D. Carlos, D. Ostrovskii, J. Rocha, Optically functional di-urethanesil nanohybrids containing Eu^{3+} ions, Chem. Mater. 16 (2004) 2530–2543.
[26] B. Yan, X.F. Qiao, Rare-earth/inorganic/organic polymeric hybrid materials: molecular assembly, regular microstructure and photoluminescence, J. Phys. Chem. B 111 (2007) 12362–12374.
[27] P. Tien, L.K. Chau, Novel sol-gel derived material for separation and optical sensing of metal ions. Propylethylenediamine triacetate-functionalized silica, Chem. Mater. 11 (1999) 2141–2147.
[28] A. Malik, Advances in sol-gel based columns for capillary electrochromatography: sol-gel open-tubular columns, Electrophoresis 23 (2002) 3973–3992.
[29] A.M. Siouffi, Silica gel-based monoliths prepared by the sol-gel method: facts and figures, J. Chromatogr. A 1000 (2003) 801–818.
[30] O.L. Malta, M.A. Couto dos Santos, L.C. Thompson, N.K. Ito, Intensity parameters of 4f-4f transitions in the $Eu(dipivaloylmethanate)_3$ 1,10-phenanthroline complex, J. Lumin. 69 (1996) 77–84.
[31] O.L. Malta, H.F. Brito, J.F.S. Menezes, F.R. Goncaülves e Silva, S. Alves Jr., F.S. Farias Jr., A.V.M. de Andrade, Spectroscopic properties of a new light-converting device $Eu(thenoyltrifluoroacetonate)_3$ 2(dibenzyl sulfoxide). A theoretical analysis based on structural data obtained from a sparkle model, J. Lumin. 75 (1997) 255–268.
[32] L.D. Carlos, Y. Messaddeq, H.F. Brito, R.A. Sá Ferreira, V. de, Zea. Bermudez, S.J.L. Ribeiro, Full-color phosphors from europium(III)-based organosilicates, Adv. Mater. 12 (2000) 594–598.
[33] R.A. Sá Ferreira, L.D. Carlos, R.R. Goncaülves, S.J.L. Ribeiro, V. de, Zea. Bermudez, Energy-transfer mechanisms and emission quantum yields in Eu^{3+}-based siloxane-poly(oxyethylene) nanohybrids, Chem. Mater. 13 (2001) 2991–2998.
[34] P.C.R. Soares-Santos, H.I.S. Nogueira, V. Felix, M.G.B. Drew, R.A. Sá Ferreira, L.D. Carlos, T. Trindade, Novel lanthanide luminescent materials based on complexes of 3-hydroxypicolinic acid and silica nanoparticles, Chem. Mater. 15 (2003) 100–108.
[35] E.E.S. Teotonio, J.G.P. Espinola, H.F. Brito, O.L. Malta, S.F. Oliveria, D.L.A. de Foria, C.M.S. Izumi, Influence of the N-[methylpyridyl]acetamide ligands on the photoluminescent properties of Eu(III)-perchlorate complexes, Polyhedron 21 (2002) 1837–1844.
[36] S.J.L. Ribeiro, K. Dahmouche, C.A. Ribeiro, C.V. Santilli, S.H.J. Pulcinelli, Study of hybrid silica-polyethyleneglycol xerogels by Eu^{3+} luminescence spectroscopy, J. Sol-Gel Sci. Technol. 13 (1998) 427–432.
[37] M.H.V. Werts, R.T.F. Jukes, J.W. Verhoeven, The emission spectrum and the radiative lifetime of Eu^{3+} in luminescent lanthanide complexes, Phys. Chem. Chem. Phys. 4 (2002) 1542–1548.
[38] C.Y. Peng, H.J. Zhang, J.B. Yu, Q.G. Meng, L.S. Fu, H.R. Li, L.N. Sun, X.M. Guo, Synthesis, characterization, and luminescence properties of the ternary europium complex covalently bonded to mesoporous SBA-15, J. Phys. Chem. B 109 (2005) 15278–15287.